Computer Simulation of the Static and Dynamic Properties of a Polymer Chain

David Ceperley

National Resource for Computation in Chemistry, Lawrence Berkeley Laboratory, Berkeley, California 94720

M. H. Kalos

Courant Institute of Mathematical Sciences, New York University, New York, New York 10012

Joel L. Lebowitz*

Departments of Mathematics and Physics, Rutgers University, New Brunswick, New Jersey 08903. Received December 16, 1980

ABSTRACT: We have carried out computer simulations of the statics and dynamics of an isolated model polymer chain with excluded volume in a solvent acting as a heat bath. We find that the distribution function for the separation of a pair of beads scales as the number of beads N to the power ν and that edge effects are small. The dynamical correlation functions, such as that of the end-to-end vector, scale as $N^{2\nu+1}$ with $\nu \simeq 0.6$. The results of a dynamical lattice polymer model are shown to be consistent with the present results if one adjusts the time scales in such a way that the center of mass diffuses at the same rate in the two models. The relaxation of the stress tensor is shown to be quite similar to that of the Rouse model. Finally, it is shown that edge effects are much more pronounced in the diffusive motion of the individual beads, there being a skin comprising about 30% of the total polymer, where bead motion is relatively quicker.

1. Introduction

When a solution of macromolecules is sufficiently dilute, the interactions between polymer chains can be neglected.[1,2] A good model for this system then consists of one chain in a sea of solvent. We describe here some equilibrium and kinetic properties obtained by numerically simulating the dynamical evolution of such chains. A preliminary account of this work appeared earlier.[3]

Computer calculations, and in particular Monte Carlo methods, have been used previously to find the equilibrium properties of a single chain, especially for lattice models. Our results are in agreement with other calculations in showing that when there are excluded volume interactions between elements of the chain, the size of the chain grows as N^ν, where N is the number of beads and $\nu \sim 0.6$. This agrees in turn with theories proposed by Flory and others[1,2] that the exponent should be universal,[4] independent of the details of the excluded volume interaction, and the same for lattice and continuum systems.

On the other hand, dynamical calculations of lattice models have not shown the same kind of agreement with theoretical predictions.[5] The models used have subsequently been criticized[6] on grounds that the moves used were too restrictive. In any case, a lattice might not be able to faithfully represent the dynamics of a real polymer in which small bending and stretching motions may be important.

We therefore decided to carry out direct simulations of the dynamics of such a model chain with excluded volume in a heat bath representing a solvent. For the sake of simplicity and tractability we have neglected in this study the hydrodynamic interactions between different parts of the polymer. This interaction does not have any effect on the equilibrium properties of the chain. Its effect on the kinetics, while very important, is different from the effects of the excluded volume we shall study here[7–9] and the relative magnitude of the effects will change with circumstances. Various computer studies dealing with equilibrium and dynamic properties of continuous polymer chains have appeared recently.[10,11] They all appear to be consistent with our previous results[3] and these reported here. There has also been a new study by Kranbuehl and Verdier[12] of the kinetics of chains with excluded volume on a lattice in which additional degrees of mobility were permitted. This brought their relaxation times for $N < 50$ into agreement with our values but still left the relaxation times for larger chains slower than ours. It is our belief that this is again due to the limited repertoire of steps available on the lattice. We shall show that time is consistently defined in the two models, their results agree with ours, even for large chains.

2. Description of Model

For our present investigation we have chosen the "bead–spring" model to represent the polymer chain. The chain contains N beads with coordinates $R = \{r_i, 1 \le i \le N\}$. Successive beads are connected by harmonic springs. A repulsive, short-range excluded volume interaction $\Phi(r)$ acts between all pairs of beads. The total potential energy of the chain is

$$U(R) = \sum_{i=1} \tfrac{1}{2}\kappa(\mathbf{r}_i - \mathbf{r}_{i+1})^2 + \sum_{i<j}\Phi(|\mathbf{r}_i - \mathbf{r}_j|) \qquad (2.1)$$

A repulsive Lennard-Jones 6–12 potential was chosen to represent the excluded volume interaction

$$\Phi(r) = 4\epsilon[(\sigma/r)^{12} - (\sigma/r)^6 + 1/4] \qquad r \le r_c$$

$$\Phi(r) = 0 \qquad r \ge r_c \qquad (2.2)$$

where $r_c = 2^{1/6}\sigma$. This potential is continuous and has a continuous first derivative but is stiff enough for small r that the effective excluded volume depends only weakly on ϵ. On the other hand, $\epsilon = 0$ or $\sigma = 0$ corresponds to the Rouse model,[1,13] i.e., to an ideal chain.

The energy $U(R)$ in (2.1) is to be thought of as modeling the effective, purely repulsive, interactions between polymer segments in a good solvent.[1,2] The equilibrium distribution of a chain in such a solvent is $Z^{-1} \exp[-\beta U(R)]$, with β a parameter playing the role of a reciprocal temperature. The essential feature of universality is that many properties of the chain are, for large N, independent of the details of $U(R)$.

We have chosen our units of length to be σ and let $\beta\kappa = 2$ and $\beta\epsilon = 0.1$. With these parameters the average bead separation in equilibrium is 1.45. While it is possible for

two sections of the chain to cross, such events are very unlikely and presumably do not affect the results significantly.

Following Kirkwood, Rouse, and Zwanzig,[7,13] we assume that the velocity of the polymer is proportional to the forces acting on it at any time; this is the high-viscosity limit in which inertial terms are neglected. Neglecting also hydrodynamic forces, we then have for the velocity of the *j*th bead at time *t*

$$\mathbf{v}_j(t) = -\beta D \vec{\nabla}_j U(R) + \mathbf{W}_j(t) \qquad (2.3)$$

Here β is the reciprocal temperature of the solvent, D is the diffusion constant of a monomer, and W is a Gaussian fluctuating "Langevin force" (due to the solvent) with mean $\langle \mathbf{W}_j(t) \rangle = 0$ and covariance $\langle W_i(t_1) W_j(t_2) \rangle = 6D\delta(t_1 - t_2)\delta_{ij}$. Equation 2.3 leads to the Smoluchowski equation[14] for the time evolution of the polymer probability density $f(R,t)$

$$\partial f(R,t)/\partial t = D\sum_{j=1} \vec{\nabla}_j [\vec{\nabla}_j f(R,t) + \beta f(R,t)\vec{\nabla}_j U(R)] \qquad (2.4)$$

The solution of (2.4) approaches equilibrium as $t \to \infty$:

$$f(R,t) \to Z^{-1}\{\exp[-\beta U(R)]\} \qquad (2.5)$$

3. Computational Method

The stochastic process described by (2.3) (or equivalently the solution of diffusion eq 2.4) was simulated by a special Monte Carlo scheme.

A simple simulation method would be to displace every particle at each time step by an amount proportional to the sum of the internal force and the random force. That is

$$\mathbf{r}_i(t + T) = \mathbf{r}_i(t) - \tau \beta D \vec{\nabla}_i U + \chi_i \qquad (3.1)$$

where $\langle \chi_i \chi_j \rangle = 6D\tau$. This method is not useful in the presence of strong excluded volume forces since if an overlap occurs ($|\mathbf{r}_i - \mathbf{r}_j|$ is small for some pair *ij*), the internal force on particles *i* and *j* in the next time step will be very large and they could be thrown far from the polymer. The time step τ would have to be exceedingly small to alleviate this problem. A systematic way is needed of rejecting those moves where the potential energy increases significantly.

To achieve this goal, let us first define the Green's function for the process: $G(R_0,R,t)$ is the probability density for the polymer to diffuse from the point R_0 to the point R (R_0 and R are vectors in the 3*N*-dimensional configuration space) in time *t*. In other words, G is the solution of eq 2.4 with boundary conditions

$$G(R_0,R,0) = \delta(R_0 - R) \qquad (3.2)$$

Knowledge of the Green's functions for time τ is sufficient to simulate the diffusion process in steps of τ since

$$f(R,t + \tau) = \int dR_0 \, f(R_0,t)G(R_0,R,\tau) \qquad (3.3)$$

An approximation, exact if $\vec{\nabla}U$ is constant, is

$$G_0(R_0,R,\tau) = (2\pi\tau D)^{-3N/2} \exp\left[-\frac{[R - R_0 + \tau D\vec{\nabla}U(R_0)]^2}{4D\tau} \right] \qquad (3.4)$$

Variation of $\vec{\nabla}U$ in (3.4) may lead to unphysical overlaps which can be avoided if G_0 is altered to satisfy the detailed balance condition obeyed by the exact Green's function

$$\exp[-\beta U(R_0)]G(R_0,R,t) = \exp[-\beta U(R)]G(R,R_0,t) \qquad (3.5)$$

In our simulation algorithm, we use the standard Metropolis[15] rejection technique, more familiar with equilibrium simulations but equally applicable here, to enforce

(3.5). Our simulation reads as follows:

(1) Start from a configuration $R = (\mathbf{r}_1, ..., \mathbf{r}_N)$. Permute the integers randomly. This permutation is kept fixed until all particles have been moved once.

(2) Sample a new position $\mathbf{r}_i'$ for particle *i* from 3.1 where only χ_i is nonzero.

(3) Accept this move with probability $q(R,R')$ where

$$q(R,R') = \min\left[1, \frac{e^{-\beta U(R')}G_0(R',R,T)}{e^{-\beta U(R)}G_0(R,R',T)} \right] \qquad (3.6)$$

This acceptance probability is constructed so that the transition probability density, $q(R,R')G_0(R,R',T)$ satisfies the detailed balance condition. This ensures that $f(R,t)$ obtained from the simulation satisfies (2.5).

(4) If the move is accepted, the coordinates of that particle, $\mathbf{r}_i$, are replaced by their new values, viz., $\mathbf{r}_i'$. If not, the old values are retained.

(5) Steps 1–4 are performed for each particle in the succession given by the random permutation. Time is advanced by an amount τ after each particle has had a trial move.

Because time advances whether or not the particle move is accepted, all diffusion processes will be slowed down by an amount proportional to the rejection ratio. In our simulations the time step τ is kept small enough so that the rejection ration is about 10%. With this time step it is reasonable to assume that all slow diffusive motions will be slowed down by the same factor. We can determine this scale factor since the diffusion of the center of mass can be calculated exactly from the Smoluchowski equation. It is given by

$$\int dR \, G(R_0,R,t)[\mathbf{Z}(R) - \mathbf{Z}(R_0)]^2 = 6Dt/N \qquad (3.7)$$

where $\mathbf{Z} = (1/N)\sum_{i=1}^N \mathbf{r}_i$ is the center of mass. For $\tau = 0.01$ the rejection ratio varied from 8.5% at $N = 5$ to 11.2% at $N = 63$. The slowing down of the center of mass varied from 6% at $N = 5$ to 7% at $N = 63$. All times reported below and shown in the figures have been scaled by this amount (0.94).

The computations of the force and potential are done efficiently with the use of near-neighbor tables.[16] At the start of the calculation a list of all the pairs *ij* with $|\mathbf{r}_i - \mathbf{r}_j| < r_c + 2\Delta$ is constructed. Δ is a constant which may be chosen to minimize the computer time required. Only distances for pairs in this list need be computed. The list is renewed when $\max[\mathbf{r}_i(t') - \mathbf{r}_i(t)]^2 > \Delta$. Because the excluded volume potential keeps the polymer stretched out and because diffusion times are slow, this neighbor scheme is very efficient for large polymers. However, as we shall see, all the diffusion times scale as $N^{2.2}$, and since the computation effort per move increases as N, the computer time needed to simulate a fixed number of relaxation times is proportional to $N^{3.2}$. This limits the size of polymers which can be simulated by this scheme on present computers to approximately 100.

It is possible to generalize the above method to include a hydrodynamical interaction matrix (the Oseen tensor). Then the random forces in eq 3.1 would become correlated.[1,7] This increases the computational effort considerably and has only been attempted for small chains ($N = 10$). Those results will not be reported here.

4. Static Properties of a Single Polymer

In this section we present various static properties of an isolated polymer chain, emphasizing the various ways in which the scaling behavior of lengths manifests itself. We assume implicitly that there exists a well-defined limiting behavior for very large polymers and that chains of finite
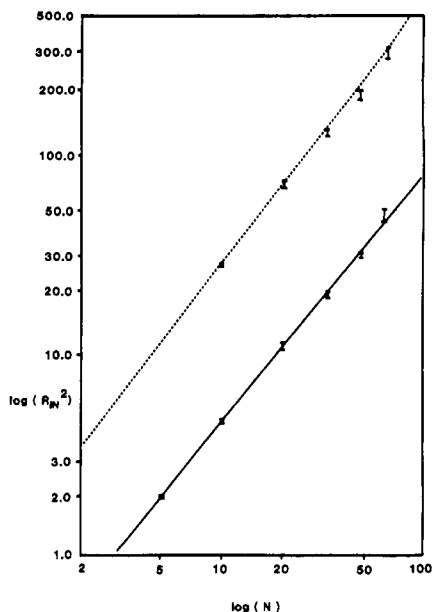
Figure 1. Mean-square end-to-end distance (dashed line) and the mean radius of gyration (solid line) vs. the number of particles.

length approximate this behavior when N is sufficiently large.[1,2]

1. Size Scaling. The customary way of demonstrating the scaling behavior of polymers is to plot the mean-square end-to-end distance vs. the number of units in the polymer chain. Such a plot is shown in Figure 1 for polymers with $N = 5-63$. We have fitted these numbers with a simple power law and find

$$\langle R_{1N}^2 \rangle \equiv \langle (\mathbf{r}_1 - \mathbf{r}_N)^2 \rangle \approx (0.92 \pm 0.02) a^2 (N - 1)^{1.21 \pm 0.03}$$

$$(4.1)$$

where $a^2 = 2.1$ is the mean-square link length in our units.

The radius of gyration is also plotted in Figure 1 and obeys a similar relationship

$$G^2 = \frac{1}{N} \sum_{i=1}^{N} \langle (r_i - \mathbf{Z})^2 \rangle \approx (0.11 \pm 0.05) a^2 (N - 1)^{1.12 \pm 0.02}$$

$$(4.2)$$

where $\mathbf{Z}$ is the center of mass of the chain. A more detailed analysis of computer results on a model chain with fixed links of length a and excluded volume interaction of the same form as ours was made by Webman et al.[10b] By taking explicitly into account the finite N corrections to the asymptotic power law, they obtained

$$\langle R_{1N}^2 \rangle \propto a^2 (N - 1)^{1.2} (1 - 0.5 a^{-1.8} N^{-0.2})$$

Shown in Figure 2a are the mean values of $\langle R_{ij}^2 \rangle^{1/2} \equiv \langle (\mathbf{r}_i - \mathbf{r}_j)^2 \rangle^{1/2}$ against $(i + j)/N$, the chemical center of the pair. The lines connect points of constant $i - j$; they are lines of constant chemical distance. The tip of the tree represents the end-to-end distance squared and the base represents the nearest-neighbor distances. The approximately constant value of $\langle R_{ij}^2 \rangle$ along the lines is a clear indication that the mean distance between two polymer beads is primarily a function of the chemical distance and independent of the placement of the beads within the chain. The slight bending of the branches halfway up the tree indicates that there are edge effects of the order of a few percent. The end of the polymer chain is typically surrounded by fewer polymer beads; thus it feels a smaller excluded volume force, and it has more freedom to bend than would a bead in the center of the chain. Also plotted in Figure 2b-d are $\langle R_{ij}^n \rangle^{1/n}$ for $n = -1, 4,$ and 6. Note that these graphs show the same behavior as the graph for n
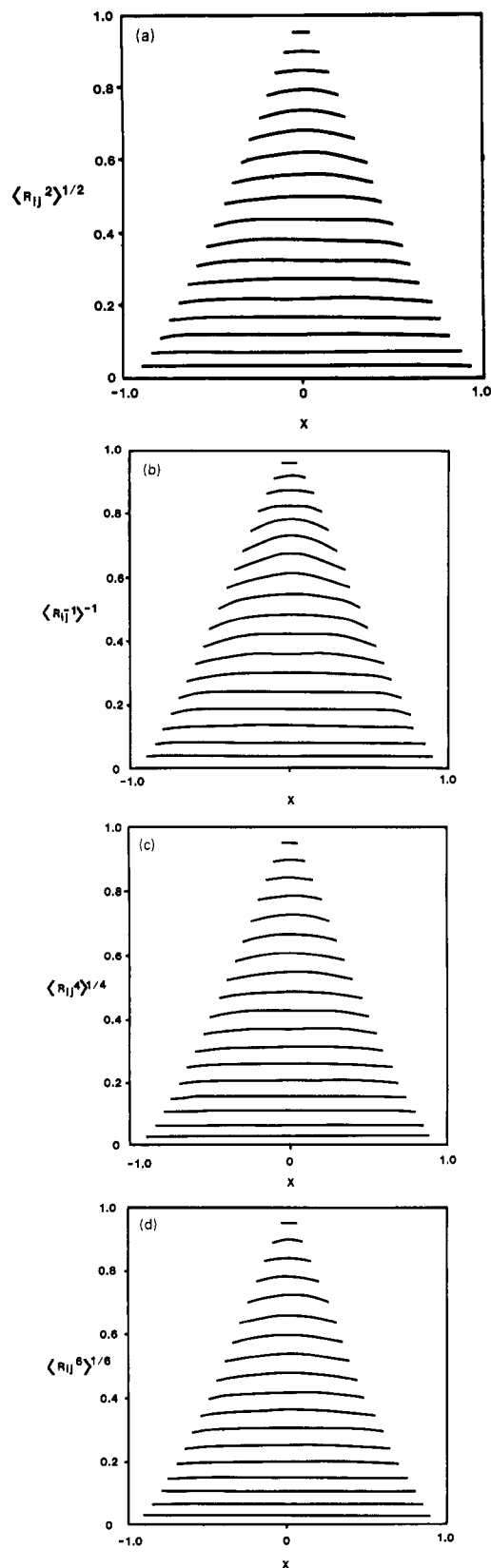
Figure 2. Average values of four moments of R_{ij} vs. the relative distance, x, from the center of the chain for a chain with 20 beads, where $x = (i + j - 21)/19$. The lines connect points of constant chemical distance $(i - j = \text{constant})$. The vertical axis is in units of $\langle R_{1,20}^M \rangle^{1/M}$. Hence the bottom of the tree represents moments of adjacent beads.

$= 2$. This indicates that the distribution of the R_{ij}'s is a universal function of $R_{ij}/\langle R_{ij}^2 \rangle^{1/2}$ for long chains. We have checked the behavior of this tree as N changes and found

Table I
Statistical Properties of Our Model[a]

N	T	$\langle R_{1N}{}^2 \rangle$	$\langle G^2 \rangle$	$\langle T_1{}^2 \rangle / \langle G^2 \rangle$	$\langle T_2{}^2 \rangle / \langle G^2 \rangle$
5	5×10^3	10.35 ± 0.05	1.929 ± 0.012	0.037	0.166
10	5×10^3	27.8 ± 0.03	4.65 ± 0.04	0.051	0.159
20	7.5×10^3	70 ± 4	11.0 ± 0.5	0.053	0.157
33	10^4	125 ± 6	19.9 ± 0.6	0.054	0.162
48	11×10^4	197 ± 14	31 ± 1.5	0.057	0.176
63	8×10^3	321 ± 40	48.6 ± 5	0.050	0.157

[a] N is the number of beads, T is the total simulation time (in units of σ^2/D), R_{1N} is the end-to-end distance. G is the radius of gyration, and $T_1{}^2$ and $T_2{}^2$ are the smallest and second eigenvalues of the moment of inertia tensor.

that, in appropriate reduced units, it has the same shape; we have not studied the effect of different potentials as a direct observation of universal behavior (see, however, Webman et al.[10b] and references therein).

2. Characteristic Shape. The average shape of a chain is another quantity which should be independent of the size of the chain. The simplest information about the shape is contained in the moment of inertia tensor defined by[18]

$$T_{ab} = \left\langle \frac{1}{N} \sum_{i=1}^{N} (\mathbf{r}_i - \mathbf{Z})_a (\mathbf{r}_i - \mathbf{Z})_b \right\rangle \qquad a, b = 1, 2, 3 \quad (4.3)$$

The eigenvalues of this tensor, T_i, are measures of the instantaneous width of the polymer in the three orthogonal principal axes, ordered so that $T_1{}^2 \leq T_2{}^2 \leq T_3{}^2$. Note that the sum of the three eigenvalues equals the radius of gyration. The average of $T_i{}^2/G^2$ for $i = 1$ and 2 are given in Table I. Note that they are independent of the number of beads and in fact are almost identical with the equivalent ratios found in computer simulations of the self-avoiding random walk on a lattice.[19] These results indicate that the polymer is typically shaped like a highly elongated ellipsoid of inertia, with the average principal axes being in the ratio of 1:1.8:4.0. For the non-self-avoiding random walk the corresponding ratios are 1:1.64:3.42.

3. Correlation Functions. The two-particle correlation function defined as

$$g_{ij}(r) = \langle \delta(|\mathbf{r}_i - \mathbf{r}_j| - r) \rangle \qquad (4.4)$$

contains a wealth of information about the static properties of polymers. For example, the nth moment of this probability density is just $\langle R_{ij}{}^n \rangle$, defined above. As indicated earlier, the approximate scaling behavior of the moments implies that this function should scale as

$$g_{ij}(r) \cong \langle R_{ij} \rangle^{-3} \hat{g}(r/\langle R_{ij} \rangle) \qquad (4.5)$$

where $\hat{g}(x)$ is a universal function independent of i, j, and N. We have computed this scaled function by using the configurations from our simulations. In order to increase the statistical accuracy, we have averaged over all pairs with constant chemical distance, $|i - j|$. Define

$$g_m(r) \equiv \frac{1}{N-m} \sum_{i=1}^{N-m} g_{i,i+m}(r) \qquad (4.6)$$

Plotted in Figure 3 is $\ln [R_m{}^3 g_m(r)]$ vs. the scaled squared distance $r^2/\langle R_m{}^2 \rangle$ for a 63-bead chain. The Gaussian chain appears as a straight line in this plot. There are small but significant changes with m, but all of the distribution functions show large non-Gaussian effects for both large and small distances.

The scaling behavior at small r has been calculated by renormalization group techniques by des Cloizeaux[20] for an infinitely long excluded volume chain. He finds that

$$g_{ij}(r) \propto r^{\theta_{ij}} \qquad r \ll \langle R_{ij} \rangle \qquad (4.7)$$

The exponent θ_{ij} depends on the placement of i and j in the chain. If the results of the renormalization calculation
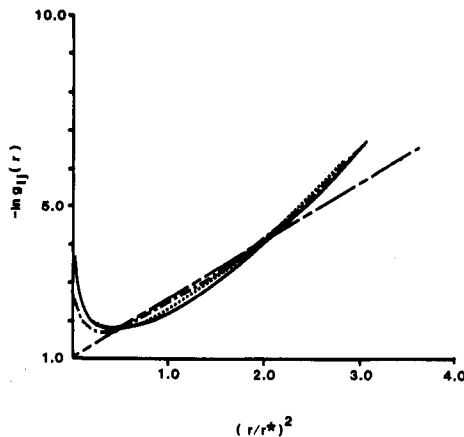

Figure 3. Logarithm of the pair distribution function for beads i and j on a chain with 63 beads as a function r^2/r^{*2}, where $r^{*2} = \langle R_{ij}{}^2 \rangle$. The distributions are averaged over all i and j that satisfy $i - j = m$, where $m = 5$ for (—), $m = 10$ for (- - -), and $m = 40$ for (-·-·). The straight line (– – –) is the corresponding curve for the ideal chain (no excluded volume interaction).
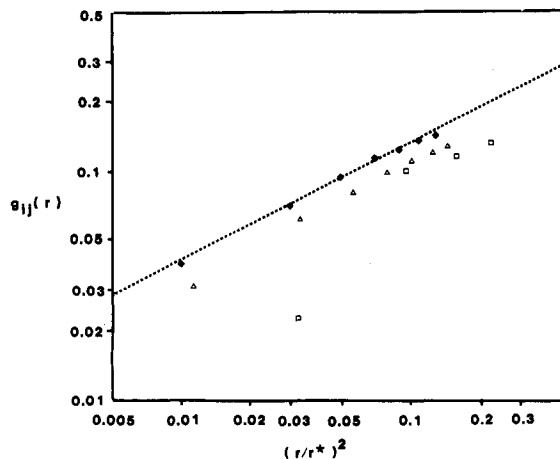

Figure 4. Probability distribution log $[g_{ij}(r)]$ vs. log $(r/r^*)^2$ for small r. The distributions are averaged over all i and j such that $i - j = m$ for a chain consisting of 48 beads. Three values of m are shown (5 ($\square$), 20 ($\triangle$), and 40 ($\blacklozenge$)). The line is the curve $g(r) = ar^{1/4}$.

apply to our bead chain, then the scaling relationship (4.5) may not be correct at small r. For three limiting possibilities the predicted exponents are

$$\theta_{ij} = 0.272 \pm 0.004 \qquad i = 0, j = N$$

$$\theta_{ij} = 0.459 \pm 0.003 \qquad 0 = i < j \ll N \qquad (4.8)$$

$$\theta_{ij} = 0.71 \pm 0.05 \qquad 0 \ll i < j \ll N$$

Figure 4 is a log–log plot of the short-distance behavior of $g_m(r)$ for several values of m. We find that each g_m has an exponent of about 0.25. This is particularly evident as $m \to N$. Since we are averaging over pairs with constant
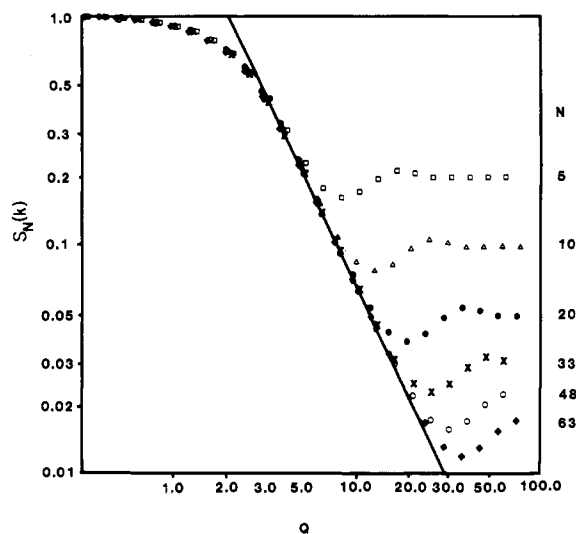
Figure 5. $S_N(k)$ vs. Q, where $Q = kN^{-\nu}$ and $\nu = 0.6$. The symbols represent the results of six different values of N (see right-hand scale). The line is $0.3Q^{-5/3}$. For large k, $S_N(k) \to 1/N$. It is seen that for $k < 2$ the curves coincide.

chemical distance, the exponent will tend to be that given by the minimum of the exponents of the different pairs, which according to eq 4.8 is that associated with pairs, one of whose members is near the end. There is no evidence, however, in our data of the much larger exponents in eq 4.8. A more extensive Monte Carlo calculation involving much larger chains would be useful.

The large-r behavior of the end-to-end distribution on the lattice has been examined by Monte Carlo by Domb[21] et al. Fisher,[22] McKenzie and Moore,[23] and des Cloizeax[20] have presented scaling arguments for the following form:

$$g_{1N}(r) \propto R_N^{-3}(r/R_N)^{0.33} \exp[-(r/R_N)^{2.50}]$$
$$r \gg R_N = \langle R_{0N}^2 \rangle^{1/2} \tag{4.9}$$

Our results are not precise enough to check eq 4.9 quantitatively but they do exhibit a significant deviation from a Gaussian (cf. Figure 3). They also indicate that whatever scaling law does apply will describe near as well as distant bead pairs. A recent study[10c] of strongly stretched continuum chains showed asymptotic behavior for large r/R_N as in eq 4.9, with an exponent of about 2.5.

The structure or scattering function is the Fourier transform of the total pair correlation function $g(r) = N^{-1}\sum_{i<j}g_{ij}(r)$

$$S_N(k) = \left\langle \frac{1}{N}\left|\sum_{j=1}^{N} e^{i\mathbf{k}\cdot\mathbf{r}_j}\right|^2 \right\rangle \tag{4.10}$$

Shown in Figure 5 is $S_N(k)$ vs. $Q = kN^{0.6}$ for various values of N. It is seen that there is a universal behavior for $1/k$ greater than a bond distance. The $S(k) \sim k^{-5/3}$ behavior for $Q \gtrsim 2$ is in accord with Edwards'[24,25] prediction of $g(r) \sim r^{-4/3}$ for $r \sim N^{0.6}$.

5. Dynamic Properties

In this section we present various time-dependent properties of the single polymer chain. We find that these properties have a scaling behavior in time. That is, the times involved in various large-scale motions of the polymer are independent of the number of monomers when properly scaled. The scaling factor can be easily determined since the diffusion of the center of mass qualifies as a large-scale motion. Let t_G be the time it takes for the center of mass to diffuse an amount equal to the radius of gyration. From eq 3.7 and 4.2 this will equal

$$t_G = \frac{0.05}{D}N^{2\nu+1} \tag{5.1}$$

To observe universal behavior, we must express all times in terms of t_G.

Time-dependent properties are commonly described in terms of correlation functions. If $H(t) \equiv H(R(t))$ is some function of the polymer chain configuration $R(t)$, then define

$$C(t;H) = \frac{\langle H(t_0)H(t_0 + t)\rangle - \langle H(t_0)\rangle^2}{\langle H(t_0)^2\rangle - \langle H(t_0)\rangle^2} \tag{5.2}$$

The averages are over an equilibrium distribution of initial values $R(t_0)$. This is represented in our simulations as an average over t_0 of one or several independent runs. The scaling behavior of the kinetics then requires that if $H(R)$ measures a global property of the polymer, then for large N, $C(tN^\alpha;H_N)$ should be independent of N, where α is a universal exponent.

In our earlier note[3] we presented results for the autocorrelation functions of the end-to-end vector, the eigenvalues of the mass tensor, the radius of gyration, and the intermediate scattering function. Here we wish to compare those results with some recent work by Kranbuehl and Verdier[12] on a dynamical lattice model and to present new results on the viscosity of the polymer chain and the relative motions of beads in the chain.

1. Kinetic Scaling in Continuous and Lattice Models. As noted in ref 3, we assumed the validity of scaling and then calculated, with a nonlinear least-squares procedure, the best value for the scaling exponent α (see Appendix A). Using the ten autocorrelation functions examined and chain lengths ranging from 5–63, we then obtained $2.04 < \alpha < 2.24$, with a typical statistical error of 0.04. We believe that the differences between the values of α as given by the least-squares fit are due primarily to the small chain lengths in our simulations and that α is indeed universal and close to $2\nu + 1$.

This result, while in satisfactory agreement with various theoretical computations, disagreed strongly with the results given in ref 5 on the time evolution of a lattice model of a polymer chain with excluded volume in which the relaxation time appeared to increase much faster with N. (Note that in the absence of any excluded volume both lattice and continuum models show behavior in which time scales as N^2.)

Following our work, Kranbuehl and Verdier[12] carried out new simulations of a dynamical lattice model. Unlike earlier work in which the configuration of the lattice polymer could change by either one or two bead moves alone, the new simulations permitted at any step either one- or two-bead moves, with the relative fraction of two-bead moves equal to p. Although this mixture of moves does indeed allow the excluded volume chain to relax much quicker than with just one type of move, their data for the largest values of N (63 beads) still appear to show a slowing down of the relaxation times by a factor of N, which is similar to that found with the more restricted lattice dynamics.

Given this situation, it seems worthwhile to find ways of making direct comparisons between the lattice model and our model. This requires in particular that we have a consistent time scale in both models. To do this we note that in continuous space, without hydrodynamical interactions, the diffusion constant is independent of the internal potential energy, while in the lattice model it may depend both on the potential and on the dynamical rules (e.g., upon the value of p). We therefore renormalize the unit of time in the two models[5] as the number of computer
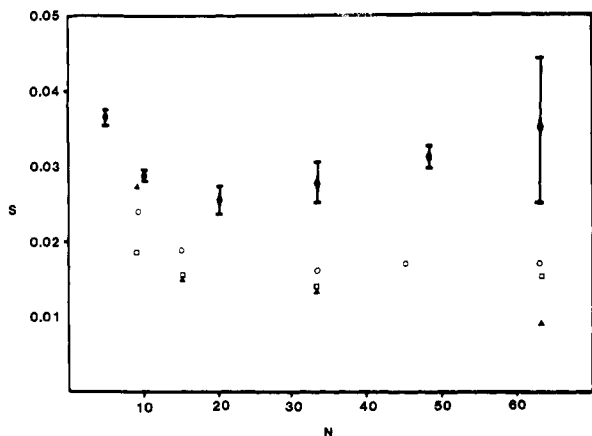
Figure 6. Ratio of the half-time of the correlation function of the end-to-end vector to the mean time for the center of mass to diffuse a distance equal to the radius of gyration as a function of the number of beads. The present calculation is shown by solid circles and error bars and the dynamical lattice simulation[12] is shown for three values of p (1.0 (△), 0.5 (○), 0.0 (▲)). p is the fraction of two-bead moves in the lattice model.

cycles needed for the mean-square displacement of the center of mass to equal a fixed multiple, say 6, of the mean-square end-to-end distance. There are sufficient data given in ref 12 to determine $t_{2,N}$, the half-time of the correlation function for the end-to-end vector, defined as

$$C(t_{2,N};R_{1N}) = \frac{1}{2} \qquad (5.3)$$

Assuming that only one exponential has survived in the correlation function, we find that for the lattice model in the units of time defined above this half-time is

$$\tau_{2,}^{NL} = \frac{R_{1N}{}^2 \ln (2a_{p,N})}{D_{p,N}\tau_p} \qquad (5.4)$$

where $a_{p,N}$, τ_p, and $D_{p,N}$ are defined in ref 12. For our model this half-time will be given by

$$\tau_{2,N}{}^c = Td_{2,N}/NR_{1N}{}^2 \qquad (5.5)$$

These quantities are plotted in Figure 6 for the two models. The most important feature to note is that these two quite different models give roughly the same ratio (about 30–50) of rotational relaxation to diffusional motion. Secondly, for our model and for the lattice model with three different values of p this ratio of times for large N appears to be constant although we cannot be too certain of this, given the rather large error bars on the present calculation. Viewed from this perspective, the lattice model computations are not as inconsistent with the generally accepted scaling behavior of time-dependent polymer properties as they seem. It would be useful to check further this question of scaling. This can be done in our model by simply increasing the length of the simulation. For the lattice model a variety of correlation functions should be examined to see if the situation of Figure 6 obtains for all such functions.

2. Viscosity of Polymer Chains. We computed the autocorrelation function of the stress tensor J_{xy}. Its Fourier transform gives the increase in the linear response to a shear wave of the chain plus solvent over the response of the pure solvent, i.e., the intrinsic viscosity:[8]

$$[\hat{\eta}(\omega)] = (\langle J_{xy}{}^2\rangle/N) \int_0^\infty dt \; e^{-i\omega t}C(t;J_{xy})$$
$$J_{xy} = \sum_{i=0}^N x_i(\partial U/\partial y_i) \qquad (5.6)$$
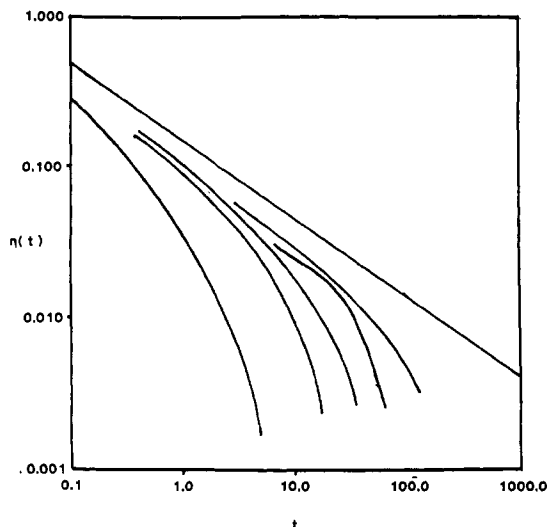
Figure 7. Logarithm of the autocorrelation function of the stress tensor vs. log (t). The straight line is for an infinitely long Rouse chain (no excluded volume) which behaves asymptotically as $t^{-1/2}$. The other five lines are fits to the simulation data for excluded volume chains, from left to right of lengths 5, 10, 20, 33, and 48.

Table II
Excess Viscosity $[\hat{\eta}(0)]$ as a Function of N, the Number of Beads per Chain[a]

N	$[\hat{\eta}(0)]$	$G^2/6$	$\langle(\vec{\nabla}U)^2\rangle$	$\langle\vec{\nabla}^2 U\rangle$	$\langle J_{xy}{}^2\rangle$	τ_m
5	0.36	0.322	43.4	44.8	30	6
10	1.4	0.77	54.1	53.0	71	12
20	2.5	1.83	57.8	56.0	152	32
33	3.0	3.2	56.7	57.1	246	60
48	7.8	5.2	58.5	57.6	371	151

[a] Relationship 5.8 asserts that $[\hat{\eta}(0)]$ should equal $G^2/6$. The agreement with our data is good only to about 40%, probably because of the large fluctuations in J_{xy} and because of the difficulty in performing the time integral. To check our program we have calculated $\langle(\vec{\nabla}U)^2\rangle$ and $\langle\vec{\nabla}^2 U\rangle$, which must be equal if averaged over the Boltzmann distribution. Also shown is $\langle J_{xy}{}^2\rangle$ and τ_m, the upper limit used in the time integral in eq 5.8.

Shown in Figure 7 are log–log plots of C for various values of N. In the Rouse model one can show that[13,26,27]

$$\lim_{N\to\infty} C(t;J_{xy}) = e^{-8t}I_0(8t)$$
$$= \frac{1}{(16\pi t)^{1/2}} + O(t^{-3/2}) \qquad (5.7)$$

where I_0 is a modified Bessel function. Our data for the excluded volume chains appear to show the same $t^{-1/2}$ dependence for times less than the slowest relaxation modes of a *finite* chain and an exponential decay for larger times.

There exists a sum rule relating the static or zero-frequency viscosity to the radius of gyration,[8] namely

$$[\hat{\eta}(0)] = (\langle J_{xy}{}^2\rangle/N) \int_0^\infty dt \; C(t;J_{xy}) = G^2/6 \quad (5.8)$$
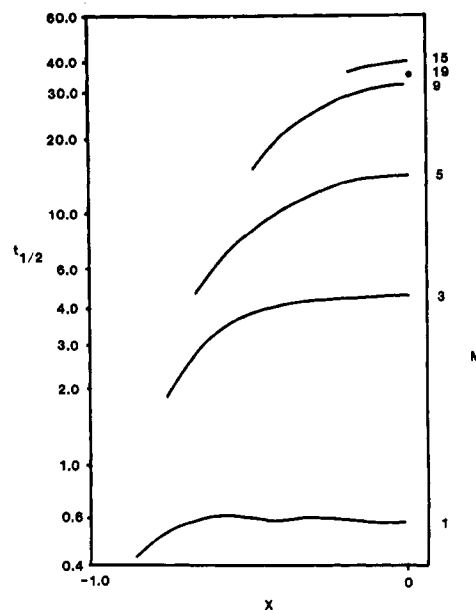
The relevant numbers are given in Table II. The agreement is to within 40%. The calculation of the integral in (5.8) is difficult from computer simulations since only three numbers (J_{xy}, J_{xz}, J_{zy}) are obtained from each configuration, and that number fluctuates greatly as the system evolves. The error is due, we believe, primarily to statis-
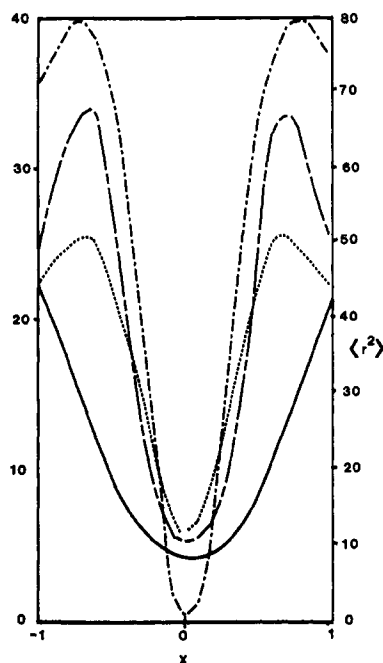
Figure 8. Relaxation time of a single bead about the center of mass for a chain of length 20 as a function of $x = (i - 10)/10$. The solid curve is $\langle (\mathbf{r}_i - \mathbf{Z})^2 \rangle$, the average square distance from the center of mass. The mean correlation time, defined as $\int dt\, C(t;\mathbf{r} - \mathbf{Z})$, is plotted as (---). The half-time of the correlation function (when $C(t_{1/2};\mathbf{r}_i - \mathbf{Z}) = 1/2$ is plotted as (--–-). The half-time for the correlation function $C(t;\mathbf{r}_i - \mathbf{r}_{21-i})$ is given by (-·-).

Figure 9. Half-time for the correlation function $C(t;\mathbf{r}_i - \mathbf{r}_j)$ plotted against x (see Figure 2) for a chain with $N = 20$. The lines connect points of constant $M = i - j$. M is given on the right-hand scale. This is the dynamical analogue of Figure 2.

tical fluctuation and secondarily to the fact that the very long time behavior has to be estimated.

3. Relative Motions of Beads. Finally, we have calculated the autocorrelation functions describing how a single bead moves with respect to the center of mass and how pairs of beads move, i.e., $C(t;\mathbf{r}_i - \mathbf{Z})$ and $C(t;\mathbf{r}_i - \mathbf{r}_j)$. Shown in Figures 8 and 9 are autocorrelations of these functions for a chain of length 20. Consider the first of these, namely, $C(t;\mathbf{r}_i - \mathbf{Z})$. It should decay in a time characteristic of the time it takes the ith particle to diffuse around the center of mass. Particles near the center of the chain are, of course, located nearer to the center of mass, as shown by the function $\langle (\mathbf{r}_i - \mathbf{Z})^2 \rangle$ plotted in Figure 8. The half-time and integral of $C(t;\mathbf{r}_i - \mathbf{Z})$ do show a deep minimum at the middle of the chain. However, near the ends of the chain the situation is quite different. The ends appear to be much more mobile than beads located in the interior of the chain. One can detect a region of the chain, comprising about 15% of each end of the polymer, where the diffusion time about the center of mass decreases as the distance to the center of mass increases. The ratio of the half-time to the integral of the correlation function expresses how nearly exponential is the decay of the correlation function. Near the ends this ratio equals (within statistical errors) the exponential value (ln 2) but it is lower near the middle of the chain. We interpret this to mean that the motion at the end of the chain has a single slow characteristic time scale. Near the center, in addition to this slow mode which will always dominate at long times, the motion is complicated by other, faster modes associated with motions about the center of mass. In Figure 9 is shown $C(t;\mathbf{r}_i - \mathbf{r}_j)$ for $N = 20$. The lines connect points of constant $i - j$. Thus this figure is the dynamical analogue of Figure 2. Although edge effects are not very important for static correlation functions, dynamically they are much more important, correlation times decreasing by

a factor of 2 if the pair of particles happens to be located near the ends.

Appendix A. Calculation of the Scaling Exponent

In this appendix we give in detail the procedure we have used for calculating the scaling exponent, α, which brings several time-dependent correlation functions into agreement. With the trajectory generated by the simulation we calculate the correlation function $C(t;H_N)$ of some property H for several values of N, using eq 5.2. The averages are taken over the entire length of the trajectory. This correlation function will depend upon the initial conditions and will fluctuate from run to run because of the finite time available for computing the average. Zwanzig and Ailawadi[28] have proposed that the variance of the estimate of the correlation function has the following form:

$$V(t,N) \equiv \langle (C - \langle C \rangle)^2 \rangle = (4\tau/T)(1 - \langle C \rangle)^2 \quad \text{(A.1)}$$

where $\tau = \int_0^\infty dt\, C(t;H_N)^2$ and T is the length of the trajectory. Our data verify their prediction within a factor of 2.

Let us assume that the scaling hypothesis is valid, namely, that there exists an α such that $C(sN^\alpha;H_N)$ is

independent of N as a function of scaled time s. Then the linear combination

$$\hat{C}(s,\alpha) = \sum_N w(t,N)C(sN^\alpha;H_N)/\sum_N w(t,N) \quad \text{(A.2)}$$

will equal the scaled correlation function. To minimize the variance of the estimate of $\hat{C}(s,\alpha)$, the weights $w(t,N)$ must be chosen so that each term in the linear combination contributes an equal variance. This implies

$$w(t,N) = 1/V(t,N) \quad \text{(A.3)}$$

The success of the scaling hypothesis can then be judged by the squared difference between the scaled averaged function and the original data:

$$\chi^2(\alpha) = s^{-1}\int_0^{s_0}\mathrm{d}s \sum_N [C(sN^\alpha;H_N) - \hat{C}(s,\alpha)]^2/V(sN^\alpha,N) \quad \text{(A.4)}$$

The best scaling exponent is that which minimizes $\chi^2(\alpha)$. In the integral in eq A.4 we have chosen s_0 to be such that for at least two values of N, $C(sN^\alpha;H_N)^2 > V(sN^\alpha,N)$; i.e., the signal is greater than the noise.

The advantages of the above procedure are that it makes no assumptions about the form of $\hat{C}(s)$, that all of the available data are used with the proper statistical weight, and that the procedure is stable (i.e., a minimum in $\chi^2(\alpha)$ is ensured).

References and Notes

(1) Flory, P. J. "Principles of Polymer Chemistry"; Cornell University Press: Ithaca, N. Y., 1953.
(2) de Gennes, P. G. "Scaling Theory of Polymers"; Cornell University Press: Ithaca, N.Y., 1979.
(3) Ceperley, D.; Kalos, M. H.; Lebowitz, J. L. *Phys. Rev. Lett.* 1978, *41*, 313.
(4) Domb, C. *Adv. Chem. Phys.* 1969, *15*, 229. McKenzie, D. S. *Phys. Rev.* 1976, *27*, 35 and references therein.
(5) Verdier, P. H.; Stockmayer, W. H. *J. Chem. Phys.* 1962, *36*, 227. Geny, F.; Monnerie, L. *Macromolecules* 1977, *10*, 1003.
(6) Hilhorst, H. J.; Deutch, J. M. *J. Chem. Phys.* 1975, *63*, 5153. Boots, H.; Deutch, J. M. *Ibid.* 1977, *67*, 4608.
(7) Kirkwood, J. G. "Macromolecules"; Gordon and Breach: New York, 1976.
(8) Stockmayer, W. H. In "Molecular Fluids"; Balian, R., Weill, G., Eds.; Gordon and Breach: New York, 1976.
(9) Freed, K. F. In "Progress in Liquid Physics"; Croxton, C. A., Ed.; Wiley: New York, 1978; p 343.
(10) (a) Webman, I.; Lebowitz, J. L.; Kalos, M.; *J. Phys. (Orsay, Fr.)* 1980, *41*, 579. (b) *Phys. Rev. B* 1980, *21*, 5540. (c) *Phys. Rev. A* 1981, *23*, 316.
(11) Helfand, E. *J. Chem. Phys.* 1971, *54*, 4651. Gottleib, M.; Bird, R. B. *Ibid.* 1976, *65*, 2467. Weiner, J. H.; Pear, M. R. *Macromolecules* 1977, *10*, 317. Fixman, M. *J. Chem. Phys.* 1978, *69*, 1527. *Ibid.* A.; *69*, 1538. Baumgärtner, A.; Binder, K. *Ibid.* 1979, *71*, 2541.
(12) Kranbuehl, D. E.; Verdier, P. H. *J. Chem. Phys.* 1979, *71*, 2662.
(13) Rouse, P. E. *J. Chem. Phys.* 1953, *21*, 1272. Zwanzig, R. *Adv. Chem. Phys.* 1969, *15*, 325.
(14) Chandrasekhar, S. *Rev. Mod. Phys.* 1943, *15*, 1.
(15) Metropolis, N.; Rosenbluth, A. W.; Rosenbluth, M. N.; Teller, A. M.; Teller, E. *J. Chem. Phys.* 1953, *21*, 1087.
(16) Cf.: Verlet, L. *Phys. Rev.* 1967, *159*, 98.
(17) Ermak, D. L.; McGammon, J. A. *J. Chem. Phys.* 1978, *69*, 1352.
(18) Solo, K.; Stockmayer, W. H. *J. Chem. Phys.* 1971, *54*, 2756.
(19) McCrackin, F. L.; Mazur, J.; Guttman, C. M. *Macromolecules* 1973, *6*, 859.
(20) des Cloizeaux, J. *Phys. Rev. A* 1974, *10*, 1665. *J. Phys. (Orsay, Fr.)* 1980, *41*, 223.
(21) Domb, C.; Gillis, J.; Wilmers, G. *Proc. Phys. Soc., London* 1965, *85*, 625.
(22) Fisher, M. E. *J. Chem. Phys.* 1966, *44*, 616.
(23) McKenzie, D. S.; Moore, N. A. *J. Phys. A* 1971, *4*, 282.
(24) Edwards, S. F. *Proc. Phys. Soc., London* 1965, *85*, 613.
(25) Cotton, J. P.; Decker, D.; Farnoux, B.; Jannick, G.; Ober, R.; Picot, C. *Phys. Rev. Lett.* 1974, *32*, 1170.
(26) Fourier transform eq 4.6 in ref 8 and convert the sum over the number of beads to an integral.
(27) Fixman, M. *J. Chem. Phys.* 1978, *69*, 1538.
(28) Zwanzig, R.; Ailawadi, N. K. *Phys. Rev.* 1969, *182*, 280.

Branch Formation in Low-Density Polyethylene

Wayne L. Mattice* and Ferdinand C. Stehling

Department of Chemistry, Louisiana State University, Baton Rouge, Louisiana 70803, and Plastics Technology Division, Exxon Chemical Company, Baytown, Texas 77520. Received February 21, 1981

ABSTRACT: Formation of short branches in low-density polyethylene (LDPE) has been investigated by using a rotational isomeric state model for the chain statistics. It is assumed that the probability of an intramolecular rearrangement of the Roedel type is proportional to the probability that reacting groups are separated by a distance $r^* \pm \Delta r$ and adhere sufficiently closely to "three in a line" geometry. Excluded-volume effects are ignored. The calculations rationalize many of the structural features observed in LDPE. They support previous proposals that ethyl groups are formed mainly by two successive Roedel-type rearrangements. The greater rate postulated by others for the second rearrangement and the measured 1:1 ratio of the two structures resulting from the second rearrangement (2-ethylhexyl and 1,3-paired ethyl branches) are predicted by the calculations. Butyl branches are calculated to be more prevalent than amyl branches. The calculations indicate that previous studies utilizing $^{13}\mathrm{C}$ NMR may have overestimated the contribution of long-chain branches to the resonances associated with branches six and longer. Our model predicts that the concentration of hexyl, heptyl, and other intermediate-length branches is unlikely to be negligibly small. Therefore, previously reported estimates for the number of long branches in LDPE based on NMR measurements are probably too high.

Low-density polyethylene (LDPE), prepared by the free radical initiated polymerization of ethylene at high ethylene pressure, is a versatile material because different physical properties can be obtained, depending on the reaction conditions used for its preparation. The number and type of short branches, which exert a strong influence on morphology and solid-state properties, are observed to vary from one sample of LDPE to the next.[1] An attractive mechanism for formation of short branches is intramolecular hydrogen atom abstraction in a cyclic intermediate.[2] In contrast, long branches can be defined as those which arise via an intermolecular hydrogen transfer.[3,4] The long branches may have a range of lengths, with an upper limit approaching the length of the main chain.

Among experimental techniques employed to characterize short-chain branching in various samples of low-density polyethylene are infrared spectroscopy,[5–9] radiol-

*To whom correspondence should be addressed at Louisiana State University.